esoc

European Space Operations Centre
Robert-Bosch-Strasse 5
D-64293 Darmstadt
Germany
T +49 (0)6151 900
F +49 (0)6151 90495
www.esa.int

DOCUMENT

S6-MF/NGRM Level 1 data description

S6-MF/NGRM Level 1 datasets

Prepared by **Ingmar Sandberg**
Space Applications & Research Consultancy

Reference **SPARC-S6MF-NGRM-L1 Data Description**
Issue/Revision **1.2**
Date of Issue **03/11/2023**
Status **Completed**

European Space Agency
Agence spatiale européenne

APPROVAL

Title S6-MF/NGRM Level 1 datasets	
Issue Number 1	**Revision Number** 1
Authors Ingmar Sandberg	**Date** 03/11/2023
Approved By	**Date of Approval**
	Digitally signed by Melanie Heil Date: 2023.11.24 12:57:24 +01'00'

CHANGE LOG

Reason for change	Issue Nr.	Revision Number	Date
Entries in Table 3 and units in Equation 4 updated	1	1	21/09/2023
New text after Eq 4 has been introduced	1	2	3/11/2023
Recommendation on the use of FPDO_1 and FPDO_3 has been added in Subsection 4.2 and in Section 5	1	2	3/11/2023

DISTRIBUTION

Name/Organisational Unit

Table of contents:

Table of figures:

Table of tables:

1 REFERENCE DOCUMENTS AND ACRONYMS

1.1 Reference Documents

[RD 1] L. Desorgher, W. Hajdas, I. Britvitch, K. Egli, X. Guo, Y. Luo, F. Chastellain, C. Pereira, R. Muff, D. Boscher, G. Maehlum, and D. Meier, “The next generation radiation monitor- NGRM,” in 2013 IEEE Nuclear Science Symposium and Medical Imaging Conference (2013 NSS/MIC). IEEE, Oct. 2013, pp. 1–6.

[RD 2] SSA P3-SWE-XXI - NGRM Data Processing,TN4: NGRM extended response functions, Reference: SE2S-NGRM-TN4

[RD 3] S. Agostinelli et al., “Geant4—a simulation toolkit,” Nuclear Instruments and Methods in Physics Research Section A: Accelerators, Spectrometers, Detectors and Associated Equipment, vol. 506, no. 3, pp. 250–303, Jul.2003.

[RD 4] I. Sandberg et al., "Data Exploitation of New Galileo Environmental Monitoring Units," in IEEE Transactions on Nuclear Science, vol. 66, no. 7, pp. 1761-1769, July 2019

[RD 5] S. Aminalragia-Giamini et al 2018, Artificial intelligence unfolding for space radiation monitor data, J. Space Weather Space Clim. 2018, 8, A50, https://doi.org/10.1051/swsc/2018041

[RD 6] A. Boudouridis, J. Rodriguez, B. Kress, B. Dichter, and T. Onsager, “Development of a bowtie inversion technique for real-time processing of the GOES-16/-17 SEISS MPS-HI electron channels,” Space Weather, vol. 18, no. 4, Apr. 2020.

[RD 7] SEPEM reference data set (rds) v2.X 2017a, http://test.sepem.eu/help/SEPEM RDS v2-00.zip

[RD 8] I. Sandberg, P. Jiggens, D. Heynderickx, and I. A. Daglis, “Cross calibration of NOAA GOES solar proton detectors using corrected NASA IMP-8/GME data”, Geophysical Research Letters, vol. 41, no. 3, pp. 4435- 4441, 2014d

[RD 9] Sandberg et al, “First results and analysis from ESA Next Generation Radiation Monitor unit on-board EDRS-C”, IEEE Transactions on Nuclear Science. 10.1109/TNS.2022.3160108

[RD 10] Higashio et al., The extremely high-energy electron experiment (XEP) onboard the Arase (ERG) satellite Earth, Planets and Space (2018) 70:134 https://doi.org/10.1186/s40623-018-0901-x]

[RD 11] T. Mitani et al "High-energy electron experiments (HEP) aboard the ERG (Arase) satellite", *Earth Planets Space*, vol. 70, no. 1, pp. 77, May 2018. https://doi.org/10.1186/s40623-018-0853-1

[RD 12] UNILIB http://www.mag-unilib.eu/

1.2 Acronyms

Acronyms used in this document and needing a definition can be found in:

Acronym	Definition
AI	Artificial Intelligence
BT	Bow-Tie
CBR	Case-Based-Reasoning
EDRS-C	European Data Relay Satellite C
EPT	Electron Proton Telescope
ESA	European Space Agency
EDSS	Electron Detector Stacked System
ESOC	European Space Operations Centre
ESTEC	European Space Research and Technology Centre
HEO	Highly Elliptic orbit
HEP	high-energy electron experiment
GA	Genetic Algorithm
GenCORUM	Genetic Correlative Unfolding Method
GP	Ground Processor
GTO	Geo Transfer Orbit
FEDO	Omni-directional Differential Electron Flux
FEIO	Omni-directional Integral Electron Flux
FPDO	Omni-directional Differential Proton Flux
MTG-I 1	Meteosat Third Generation-Imager 1
NGRM	Next Generation Radiation Monitor
ODI	Open Data Interface
PODC	Payload Operation Data Centre
RB	Radiation Belts
REM	Radiation Environment Monitor
RF	Response Function
SDSS	Solid Detector Stacked System
S6-MF	Sentinel-6 Michael Freilich
SEP	Solar Energetic Particle
TAS	Thales Alenia Space
TN	Technical Note
XEP	extremely high-energy electron experiment

Table 1: Acronyms

2 INTRODUCTION

2.1 Purpose

This document describes the main characteristics of the released Sentinel-6 Michael Freilich (S6-MF) NGRM Level 1 Version 1 datasets and highlights the methods used for their derivation.

2.2 Background

ESA Next Generation Radiation Monitor (NGRM) was designed to measure protons from 2 MeV up to 200 MeV and electrons from 100 keV up to 7 MeV. NGRM development started within a consortium led by TAS-CH space (former RUAG space), together with Paul Scherrer Institute (PSI), Office National d'Etudes et de Recherches Aerospatiales (ONERA), EREMS, and Integrated Detector Electronics AS (IDEAS). The first unit was placed on-board the Geostationary (GEO) European Data Relay System Satellite-C (EDRS-C), launched on August of 2019, the second was placed on board the Low Earth Orbit (LEO) Sentinel-6 Michael Freilich (S6-MF) satellite, launched on November 2020 and the third one is on board the first Meteosat Third Generation-Imager 1 (MTG-I 1), at GEO, launched on 13 December 2022. Within "SSA P3-SWE-XXI NGRM Data Processing activity", SPARC led a consortium that included Solenix, SE2S and DHConsultancy, as external service provider, aiming to the design and the implementation of the NGRM Ground Processor. The performed developments included, among others, the derivation of the response functions for the NGRM units and the development and implementation of methods for the derivation of NGRM Level 1 flux products. The present document focus on the NGRM unit on-board S6-MF. It should be noted that this unit is also termed as REM (Radiation Environment Monitor).

2.3 ESA NEXT GENERATION RADIATION MONITOR

The NGRM unit includes the electron and the stacked detector subsystems [RD 1] . The electron detector subsystem (EDSS) provides measurements in 16 channels while the stacked (proton) detector subsystem (SDSS) in 10 channels. EDSS is a circular strip detector made of 16 strips covered by a collimator made by an aluminium part on the bottom and covered by a copper cone on the top. The collimator is embedded in the aluminium housing acting as a field-of-view limiter and side shielding against particles coming from other directions. The aluminium part of the collimator is made by a concentric succession of 12 circular stairs with different thicknesses. Each silicon circular strip is bonded to an ASIC high gain channel where particles are counted when their deposited energy is within the range fixed by the low and high detection thresholds of the corresponding ASIC channel. SDSS consists of a stack of 7 Silicon cylindrical diodes separated by aluminium and tantalum degraders of different thicknesses. The diodes and the absorbers are shielded from the side by copper and aluminium cylinders. The aperture of the detector has a half opening angle of 40 degrees. Energetic particles coming from the top through the aperture cone are detected by ionization in a diode if they have sufficient minimum energy to cross all the previous

degraders and diodes. The ionization current generated by a particle crossing the diode is processed by ASIC electronic circuits.

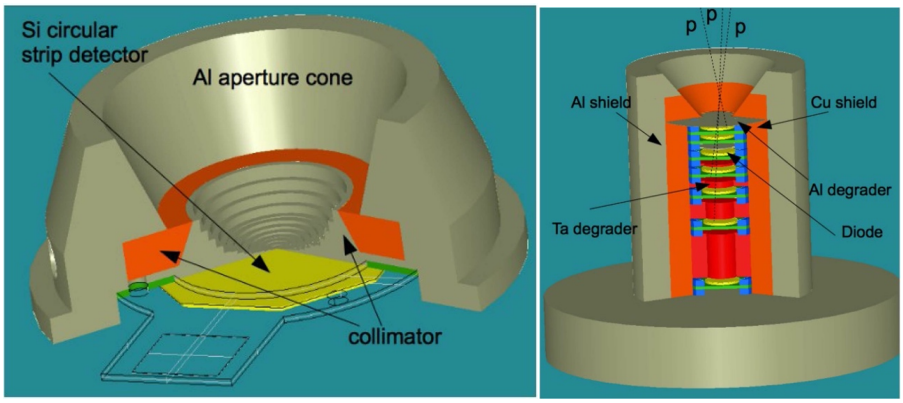

Figure 1: Model of the NGRM electron detector (left) and stacked detector (right).

3 CALIBRATION OF NGRM UNIT

The electron (proton) response functions (RF) of the EDSS (SDSS) of NGRM on-board S6-MF have been derived [RD 2] on the basis of experimental and GEANT4 [RD 3] numerical calibrations. The response curves were numerically derived, and they re-adjusted using the experimental results of the unit's experimental calibrations that took place at the Proton Irradiation and at the Electron Monochromator Facilities at Paul Scherrer Institute in Switzerland. The curves of the finalized response functions that were used for the calibration of the s6-MF/NGRM measurements and the derivation of the Level 1 flux products are presented below.

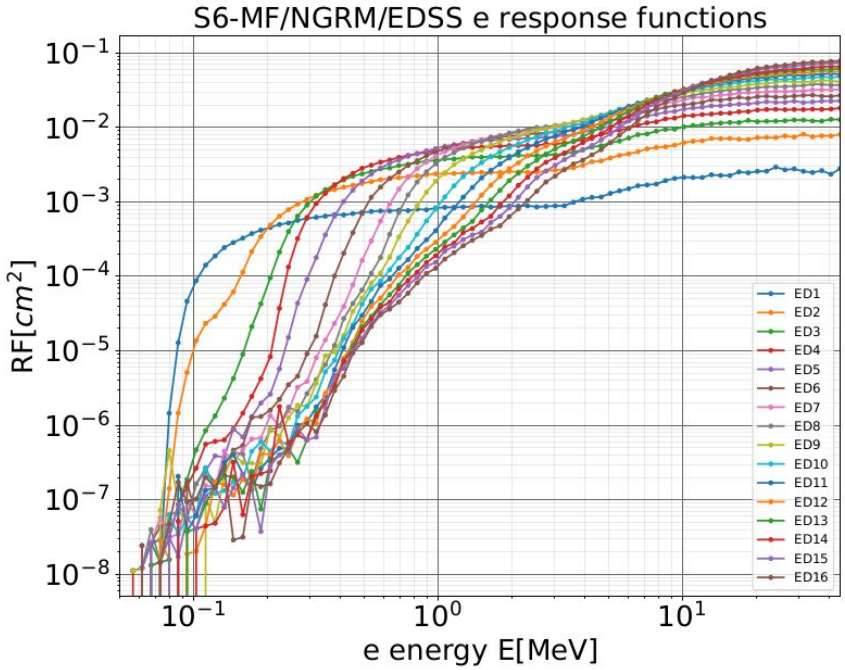

Figure 2: Omni-directional electron response functions of S6-MF/NGRM Electron Detector (ED) channels.

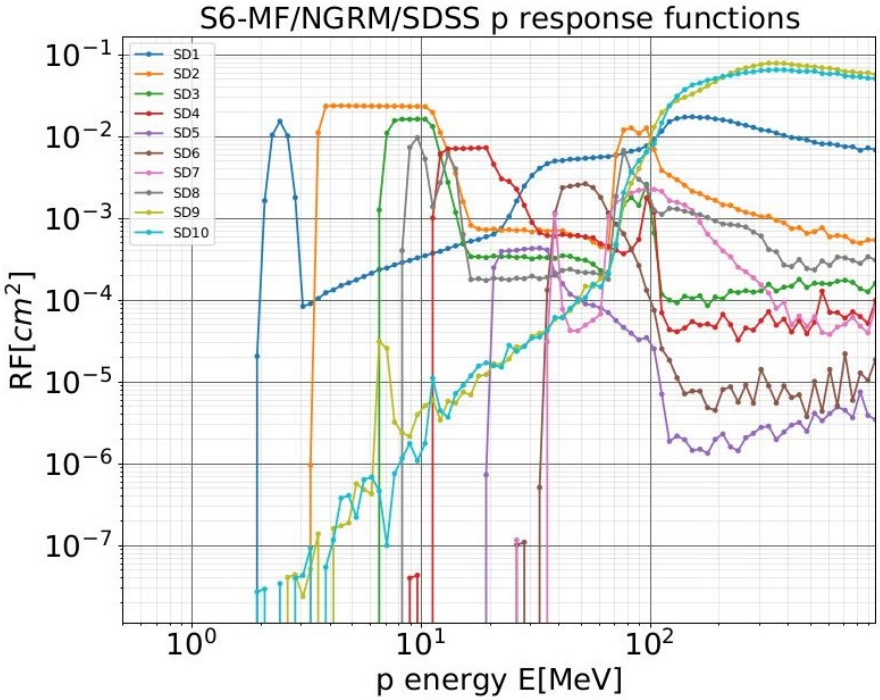

Figure 3: Omni-directional proton response function of s6-MF/NGRM Stacked Detector (SD) channels.

4 DATA CALIBRATION

The conversion of count data to calibrated energetic particle fluxes, corresponds to the derivation of solutions of the one-dimensional unfolding problem where the response (measurements) *C* of a detector is the result of the convolution of the incident differential particle fluxes *f(E)* with the response function *RF(E)* of the unit.

$$C = \int_0^\infty f(E)\, RF(E)\, dE \qquad \textbf{Equation 1}$$

For the derivation of S6-MF NGRM Level-1 fluxes two different methodologies were employed. For the calculation of proton differential fluxes and electron integral fluxes, simple multiplicative scaling factors were derived and applied, following using the Bow-Tie (BT) analysis [RD 4]. The BT analysis allows the derivation of a scaling factor for the conversion of the detector's count rates to flux products for an energy value that minimizes the uncertainties expected at the encountered space radiation environment. For the calculation of electron differential fluxes, the Genetic Correlative Unfolding Method (GenCORUM) was applied. The GenCORUM [RD 5] is an artificial intelligence method which employs a Cased-Based Reasoning (CBR) process coupled with a Genetic Algorithm (GA).

4.1 Electron Integral Flux Dataset: Level 1 Version 1

For the calculation of electron integral fluxes, a data-driven variant [RD 4] of the commonly used Bow-Tie (BT) analysis approach was implemented. For the sampling of electron radiation environment at LEO environment the differential electron flux measurements from the data of XEP [RD 10] and HEP [RD 11] units on-board JAXA Arase mission were used. This electron differential flux dataset was selected due to its extensive energy range and to its L-shell coverage. The GTO Arase electron flux measurements were initially fitted, using a power law with an exponential cutoff, and the resulting dataset, i.e. $f(E,t)$ was used for the derivation of suitable NGRM scaling factors following the procedure below.
For each ED channel, distributions of geometric factors $GF(E_i, t)$ for different energies E_i were derived through the integration of the training differential flux spectra with the corresponding response function divided by the training integral flux spectra:

$$GF(E_i, t) = \frac{\int_0^\infty RF(E)\, f(E) dE}{\int_{Ei}^\infty f(E) dE} \qquad \textbf{Equation 2}$$

A characteristic bow-tie energy was determined for each channel as the optimum value that minimizes the mean squared error of the distribution of the logarithmic values of the geometric factors. This approach was applied to the first 10 out of 16 ED channels. For the last 6 channels, it was found that the nominal bow-tie energy values were very close with each other, as expected due to the similar characteristics of the corresponding electron response curves. Thus, for the last 6 ED channels, the standard BT approach was discarded and the scaling factors for these channels were determined for pre-selected energies within the range of 1.2-1.7 MeV. This approach permits the extension of the energy range of the derived integral flux spectra - up to 1.7 MeV - at the cost of increasing uncertainties of the derived integral flux values. In all cases, the median value of the resulted distributions was

selected for the definition of the scaling factor, i.e., $SF_{50}=1/median(GF(E_{BT}))$, for each channel.

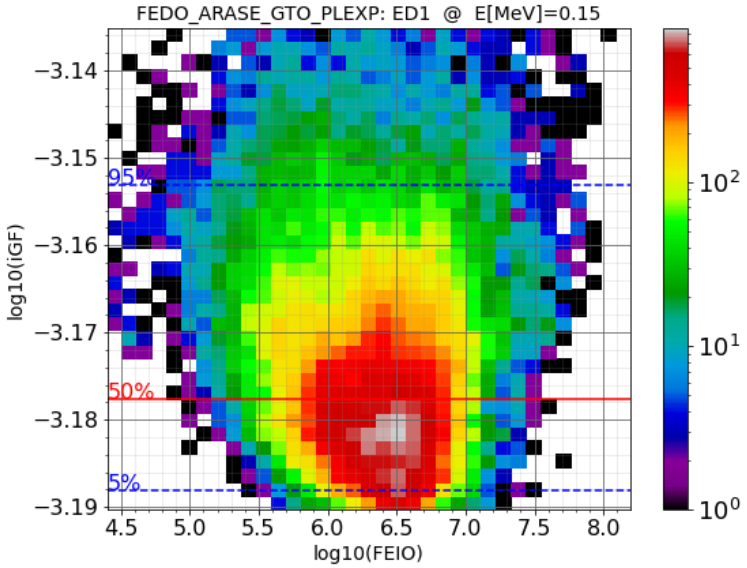

Figure 4: Histogram of the distribution of the geometric factors for the first channel at E=0.15 MeV, derived using Equation 1. The horizonal lines denote selected percentiles of the geometric factors.

For a quantitative evaluation of the uncertainties of the derived electron flux which are attributed to the selection of the median value of the distribution of the geometric factors – as derived by using as sample the GTO HEP/XEP Arase dataset – we have calculated the uncertainties using the extremes in the sampled electron radiation environment measurements.

The table below summarizes the analysis and the results associated to the derivation of the S6-MF NGRM electron integral fluxes - which have been introduced in the Level 1 Version 1 NGRM dataset – and includes also the relative differences between the 1% and the 99% percentiles of the scaling factor distributions with respect to the median value (50% percentile) which was used for the derivation of the integral electron fluxes.

Table 2: Characteristics of L1 V1 S6-MF/NGRM electron integral flux dataset.

Flux Bin	EDSS channel	FEIO_ENERGY [MeV]	SF50	(SF1-SF50)/SF1	(SF99-SF50)/SF99
1	1	0.15	1505	0.03	-0.10
2	2	0.25	524	0.03	-0.12
3	3	0.35	303	0.04	-0.14
4	4	0.4	225	0.04	-0.12
5	5	0.5	202	0.04	-0.14
6	6	0.65	177	0.04	-0.15
7	7	0.8	149	0.05	-0.16
8	8	0.9	149	0.05	-0.18
9	9	1.0	167	0.06	-0.25
10	10	1.1	214	0.08	-0.37
11	11	1.2	249	0.11	-0.49
12	12	1.3	279	0.14	-0.65

13	13	1.4	302	0.18	-0.86
14	13	1.5	293	0.26	-1.23
15	15	1.6	293	0.32	-1.53
16	16	1.7	275	0.41	-1.97

The negative sign in the last column indicates an overestimation of the BT flux products with respect to the 0.99 percentile.

The calculation of the integral electron fluxes FEIO requires the application of the following scheme,

$$FEIO[FEIO_{ENERGY}] = \frac{SF_{50} \times ED_{COUNTRATE}}{4\pi} \; [cm^2 \sec str]^{-1} \qquad \textbf{Equation 3}$$

which takes place on-the-fly as soon as raw ED measurements become available at NGRM Ground Processor.

- The FEIO dataset is accompanied by a FEIO_QUALITY variable which indicates the presence of proton contamination in the electron flux dataset. This variable receives the values 0 and 1 depending on the L-shell value across S6-MF orbit and on the count-rate measurements of SD_2, namely the second channel of the SDSS detector. FEIO_QUALITY=0 indicates the absence of proton contamination and FEIO_QUALITY=1 indicates the presence of proton contamination.

OBS: The measurements of S6-MF/NGRM/EDSS ED7 and ED14 channels are characterized by lower intensities with respect to their neighboring ones, an inconsistent finding with respect to the corresponding response curves.

4.2 Proton Differential Flux Dataset: Level 1 Version 1

For the calculation of proton differential fluxes, a BT analysis of NGRM SDSS proton responses was applied using the Solar Energetic Particle Environment Modelling (SEPEM) reference dataset (SEPEM RDS) [RD 7] as a training dataset. SEPEM is based on NOAA GOES proton flux measurements cross-calibrated by [RD 8] using as reference the IMP-8 Goddard Medium Energy experiment.

The presence of strong contamination in the outputs of SD channels 1, 9 and 10 does not permit at all the use of these measurements. The presence of electron contamination in channel SD8 allows its use only for SPE measurements outside the trapped electron radiation environment.

In what follows we summarize the results of the BT analysis for SD channels which provide the proton differential flux products in Level 1 dataset.

Table 3: Characteristics of S6-MF/NGRM proton differential flux dataset.

Flux Bin	SDSS channels	FPDO Energy [MeV]	SF_50	(SF1-SF50)/SF1	(SF99-SF50)/SF99
1	2	5.0	8.97	0.02	-0.10
2	3	9.0	12.02	0.006	-0.07
3	8	10	37.7	0.05	-0.13
4	4	15	14.48	0.01	-0.06
5	6	50	14.20	0.003	-0.05
6	7	73	9.67	0.001	-0.15

The calculation of the proton differential fluxes FPDO requires the application of the following scheme,

$$FPDO[FPDO_{ENERGY}] = \frac{SF_{50} \times SD_{COUNTRATE}}{4\pi} \; [cm^2 MeV \sec str]^{-1} \qquad \textbf{Equation 4}$$

which takes place on-the-fly as soon as raw SD measurements become available at NGRM Ground Processor.

As mentioned above, the scaling factors were derived to optimize the derivation of proton fluxes from SPEs. To evaluate the range of uncertainties in the derived fluxes from measurements from the inner proton belt, we have run an analysis for the SD channels for the BT energies of Table 3 using proton measurements from PROBA -V/EPT.

The table below presents the relative differences between the 50%, the 1% and the 99% percentiles of the scaling factor distributions for the sampled (inner belt) environment with respect to the median value (50% percentile) which was used for the derivation of the differential proton fluxes based on the sampling of the SPE environment (cf. Table 3).

Table 4: Relative differences of the scaling factor distributions for the sampled (inner proton belt) environment with respect to the scaling factor used for the derivation of the S6/NGRM proton flux dataset

Flux Bin	SDSS channels	FPDO Energy [MeV]	(SF50_RB-SF50_SPE)/SF50_RB	(SF1_RB-SF50_SPE)/SF1_RB	(SF99_RB-SF50_SPE)/SF99_RB
1	2	5.0	**-0.74**	-0.13	**-1.22**
2	3	9.0	-0.11	0.0005	-0.20
3	8	10	**-1.00**	-0.16	**-1.70**
4	4	15	-0.28	0.07	-0.39
5	6	50	-0.02	0.004	-0.05
6	7	73	-0.22	-0.001	-0.45

OBS: The relative differences for the first and the third proton flux bin are significantly large. The use of the derived BT proton fluxes - for the trapped proton measurements - at 5 and 10 MeV should be avoided.

4.3 Electron Differential Flux Dataset: Level 1 Version 1

The application of any direct re-scaling approach results to uncertainties in the derivation of differential particle fluxes. This is especially true for energies above 1.5 MeV in the case of NGRM units where the electron response functions are of integral-type. Thus, for the derivation of the electron differential fluxes, the GenCORUM method was adopted. GenCORUM is an artificial intelligence method which combines two different methodologies; a Case-Based-Reasoning (CBR) process and a Genetic Algorithm (GA). The CBR process performs an initial "rough" unfolding producing particle spectra and this output is forwarded to the GA which fine-tunes each spectrum independently producing the final unfolded particle fluxes.
During the CBR process, a virtual "library" is created by folding virtual electron flux spectra derived from an exponential cut-off power-law function with ED electron response functions and producing the counterpart virtual count-rates. Each count-rate measurement is correlated with the virtual library and the highest correlated virtual count-rate is found extracting its counter-part virtual flux as the match. Finally, a new intensity factor $\boldsymbol{a}$ is derived from a linear fitting of the measured and virtual count-rates. This new $\boldsymbol{a}$ is directly applied multiplicatively to the virtual flux to produce the unfolded spectrum, this is possible because a simple multiplicative change in the spectrum results in an equal change in the count-rate by definition (c.f. Equation 1). The unfolded spectrum is being used by a Genetic algorithms (GA) as an initial input. The GA is not bound by any strict analytical function offering much more versatility and potentially unfolded spectra that are much closer to reality. The GA process is depicted in the figure below. Each CBR spectrum corresponding to a measurement is randomly perturbed in order to create an initial population of N spectra that are similar but not identical.

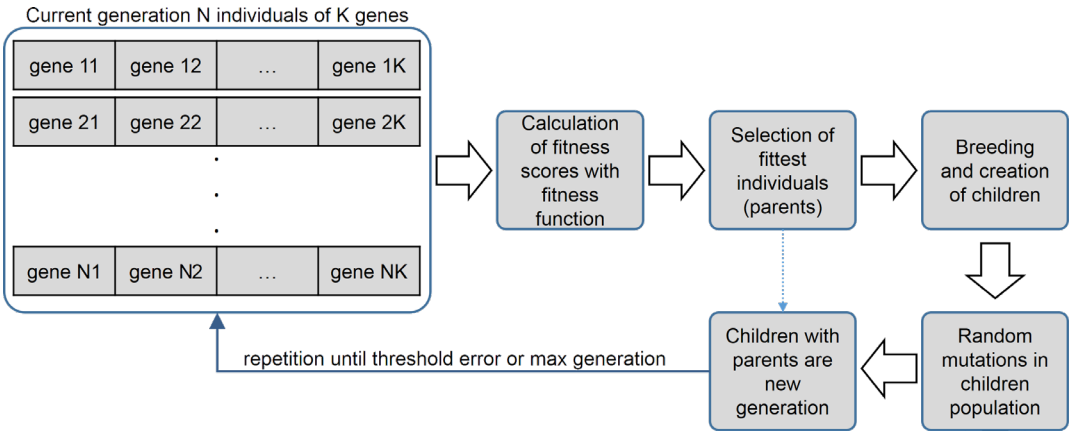

Figure 5: Diagram of the AI part of the GenCORUM process

The flux values at each energy bin are used as the "genes" in the algorithm. Each of the similar spectra is evaluated and scored in terms of how well it reconstructs the measured count-rate. The mean absolute percentage error (MAPE) is used as the fitness (score) function because it is not affected by the absolute values of the counts in the count-rate vector which can often vary by many orders of magnitude.

The process consists of four main steps:

- Fitness evaluation of the population where all the spectra are scored
- Parent selection from the population where the best performing (highest score / lowest error) spectra are selected as "parents"
- Breeding and creation of children population where the selected parents are randomly combined to create again N "children" spectra
- Random mutation of the children spectra where some of the flux values are randomly perturbed

These steps create a new population, and they are iteratively repeated, each iteration is dubbed a generation. As generations progress the overall and best performance increases and the overall and lowest error decreases. The differential electron fluxes are calculated in near real-time - as soon as NGRM raw data become available - using a GenCORUM implementation and is provided in the energy bins listed in Table 4.

Table 5: Characteristics of S6-MF/NGRM electron differential flux dataset.

Flux Bin	FEDO_ENERGY [MeV]
1	0.18
2	0.27
3	0.40
4	0.60
5	0.88
6	1.30
7	1.93
8	2.90
9	3.40
10	4.00

- The FEDO dataset is accompanied by a FEDO_QUALITY variable which indicates the presence of proton contamination in the electron flux dataset. This variable receives the values 0 and 1 depending on the L-shell value across S6-MF orbit and on the count-rate measurements of SD_2, namely the second channel of the SDSS detector. FEDO_QUALITY=0 indicates the absence of proton contamination and FEDO_QUALITY=1 indicates the presence of proton contamination.

NOTE: The measurements of S6-MF/NGRM/EDSS ED7 and ED14 channels were excluded as inputs from the GenCORUM implementation as they present, inconsistent lower intensities with respect to their neighboring ones.

5 CONCLUSIONS - WARNINGS

A limited number of evaluation studies of NGRM Level 1 flux datasets have been performed.

- S6-MF/EDSS/NGRM electron measurements have been found to be in very good consistency with the corresponding derived EDSS electron response functions. The intensity of the ED7 and ED14 measurements is lower than expected.
    - S6-MF/EDSS/NGRM electron differential fluxes present an overall consistency with third-party measurements such as Arase and PROBA-1/SREM.
    - S6-MF/EDSS/NGRM electron integral flux spectra present spectral inconsistencies for 0.8 and 1.5 MeV due to relatively low responses of ED7 and ED14 channels.

- S6-MF/SDSS/NGRM data present some inconsistencies with the corresponding SDSS proton response functions.
    - S6-MF/SDSS/NGRM proton fluxes present elevated background levels and have been found to be underestimated with respect to NOAA GOES-17 proton differential fluxes during SPEs.
    - The uncertainties in the differential proton flux datasets for 5 and 10 MeV for the inner proton belt measurements are expected to be large.
    - The eighth SDSS channel which provides the proton differential fluxes at 10 MeV is contaminated by electrons. It is recommended to be used only for SPE measurements outside regions of trapped electron radiation, e.g. at large L-shell values, i.e. L>8.

- The inclusion of FEDO_Quality and FEIO_Quality variables attempts to identify proton contamination in the electron flux products. Strong contamination by protons in the electron flux products are expected during SPEs at high magnetic latitudes.

- Data users are advised to consult the available ephemeris (ECI coordinates) and magnetic coordinate (e.g., L, MLT) variables, which have been derived using the UNILIB library [RD 12] assuming the IGRF model for the internal, and the quiet Olson-Pfitzer 1977 model for the external magnetic field components.